

Computational characterization of organic photovoltaic devices

Yuan Shang · Qikai Li · Lingyi Meng ·
Dong Wang · Zhigang Shuai

Received: 15 October 2010 / Accepted: 12 March 2011 / Published online: 30 March 2011
© Springer-Verlag 2011

Abstract We present recent progresses on applying the theoretical models and computational tools in assessing the performance of organic solar cells, especially the bulk heterojunction solar cells. Both the continuum device model and the dynamic Monte Carlo model are developed to investigate the photocurrent-voltage characteristics based on the exciton and charge carrier dynamics. Insights into key factors influencing the organic photovoltaic performances have been gained from these studies.

Keywords Organic solar cells · Photovoltaic devices · Bulk heterojunction · Continuum device model · Dynamic Monte Carlo model

1 Introduction

The development of organic solar cells has attracted tremendous attention during recent years. Because the active materials used for fabrication of these devices are polymers, soluble in most organic solvents [1–3], compared with solar cells based on inorganic semiconductors, organic solar cells have shown great potential to become flexible,

printable, low-cost and light-weight renewable energy sources [4–7], and of course, fall well into the field of chemistry, materials sciences and engineering, and electronic engineering.

In 1986, Tang first fabricated a two-layer organic solar cell [8] with a power-conversion efficiency (PCE) of 1%, the highest among all other organic-based photovoltaic devices at that time (Tang cell). The idea of introducing an interface between two organic semiconductors, namely the electron donor and acceptor, is critical in improving the photovoltaic performance. Such a donor–acceptor (DA) interface has been proved essential for excitons to dissociate efficiently into free electrons and holes that migrate through the acceptor and donor layers and produce photocurrent [9, 10].

Saricifitci et al. [4] observed that the photoinduced electron transfer from a conjugated polymer to fullerene occurs within 50 fs after photoexcitation. Following this important observation, Yu et al. [5] and Halls et al. [6] put forward the concept of bulk heterojunction (BHJ), which has attracted tremendous attention. This device structure consists of an active layer with blended electron-donating semiconducting polymers and electron-accepting fullerenes, which form interpenetrating networks [5]. When the sunlight shines on the solar cells, incident photons are absorbed to create excitons inside the energy band gap. The excitons diffuse until they arrive at a DA interface and dissociate into free charge carriers, namely electrons and holes [4]. Next, the charge carriers migrate respectively through the percolating networks toward the electrodes. Compared with the BHJ structure, a bilayer device is inefficient in respect of exciton dissociation due to the short diffusion length (typically 10–20 nm) of excitons [11], which means that only excitons generated near the DA interface are subject to dissociation. In a BHJ device, the

Dedicated to Professor Pekka Pyykkö on the occasion of his 70th birthday and published as part of the Pyykkö Festschrift issue.

Y. Shang · Q. Li · L. Meng
Key Laboratory of Organic Solids, Beijing National Laboratory for Molecular Science (BNLMS), Institute of Chemistry, Chinese Academy of Sciences, 100190 Beijing, China

D. Wang · Z. Shuai (✉)
MOE Key Laboratory of Organic Opto-Electronics and Molecular Engineering, Department of Chemistry, Tsinghua University, 100084 Beijing, China
e-mail: zgshuai@tsinghua.edu.cn

average distance between DA interfaces is reduced, and as a result, more excitons can contribute to the photocurrent, which makes the BHJ a much more promising structure than the bilayer one. Following the initial demonstration, the power conversion efficiency of the BHJ solar cells has been steadily increased to 6–7% [12, 13] and even as high as 7.7% [14] very recently, with 10% expected in the near future [1, 15, 16]. It is also anticipated that the PCE can even approach 15% with the tandem cell structure [17].

The power-conversion efficiency PCE of solar cells is defined as

$$\text{PCE} = \frac{V_{\text{OC}} \times J_{\text{SC}} \times \text{FF}}{P_{\text{in}}}, \quad (1)$$

where P_{in} is the power density of the incident light. As a result, the PCE is purely determined by the V_{OC} , J_{SC} , and FF. Simulation results with both the DMC and the device models show that the PCE is most sensitive to the nanostructure morphology and the charge carrier mobility.

V_{OC} , the maximum voltage available when the external electric current is zero, represents one of the key parameters in the solar cell devices. In order to optimize the performance of organic solar cells, the dependence of V_{OC} on several parameters is analyzed. V_{OC} is influenced by the light intensity, charge carrier mobility as well as dissociation and decay rates of photo-induced e–h pairs.

J_{SC} is the current density through the circuit when the applied voltage is zero, and as V_{OC} its optimization is of great importance to the further improvement of the efficiency of organic solar cells. Internal quantum efficiency IQE is defined as the ratio of the number of charge carriers collected by the electrode to the number of absorbed photons. Thus, J_{SC} can be written as [18]

$$J_{\text{SC}} = q \int_0^{\infty} \text{Sun}(\lambda) \times \eta_A(\lambda) \times \text{IQE}(\lambda) d\lambda, \quad (2)$$

where $\text{Sun}(\lambda)$ is the number of incident photons with wavelength λ per unit area and η_A is the ratio of the number of photons absorbed by the active layer to that of incident photons. Light intensity, mobility, and morphology can all have influences on J_{SC} and IQE.

In this account, we review recent theoretical progresses on modeling the organic solar cells and present works from our group in the theoretical characterization of the photovoltaic devices. The account is organized as follows. We first describe the theoretical methodologies for modeling organic solar cells, including both the continuum device model and the dynamic Monte Carlo model, and then we discuss the influence of parameters such as light intensity, charge carrier mobility, blend morphology, and the dissociation rate k_d as well as decay (geminate recombination) rate k_f of photo-induced electron–hole (e–h) pairs on the

photovoltaic properties such as open-circuit voltage V_{OC} , short-circuit current J_{SC} , internal quantum efficiency IQE, and power-conversion efficiency PCE. Conclusions and outlook are presented in the last section.

2 Theoretical and computational methods

2.1 Continuum device model

The continuum device model is also called the drift–diffusion model, as it captures both the drift behavior of charge carriers in an electric field and the diffusion behavior due to the gradient in charge carrier concentrations [19]. It has been applied most widely to modeling the organic light emitting diodes (OLEDs) [20, 21]. Recently, there have been more and more interests in modeling photovoltaic devices with this model [22–32]. Baker et al. [23] developed a one-dimensional device model for describing the device physics of a bilayer cell, which was found to account for the experimental results very well. In their approach, the electrons and holes are assumed to be generated directly at the interface by absorbing a fraction of incident light, instead of considering the kinetics of excitons. Koster et al. [24] have developed an equilibrium one-dimensional device model for the BHJ solar cells. The model incorporates the drift and diffusion of charge carriers, the influence of space charges on the electric field, the field- and temperature-dependent generation and the bimolecular recombination of free charge carriers. The current density–voltage (J – V) characteristics obtained for the solar cell were shown to be in excellent agreement with the experimental curves. Here, we briefly describe this method.

When an incident photon from solar emission (wavelength typically in the range of 0–800 nm) is absorbed by the polymer in the active layer of a BHJ solar cell, an exciton is created in the conjugated polymer. The exciton diffuses until it arrives at a DA interface. Upon reaching the interface, the exciton will dissociate into an e–h pair, residing on the donor and acceptor, respectively [33–36]. The ultrafast (within 100 fs) exciton dissociation, driven by the energy difference between the lowest unoccupied molecular orbitals (LUMOs) of the donor and acceptor, has a quantum efficiency of almost unity [37]. As a result, the generation rate of an e–h pair is the same as that of the exciton which is determined by the solar spectrum and absorption of the active layer of solar cells. The bound e–h pair may either dissociate into free carriers with a rate k_d or geminately decay to the ground state with a rate k_f . Therefore, the annihilation of e–h pairs is a competition between the dissociation and the decay of e–h pairs. The probability of e–h pair dissociation is given by [38]

$$P = k_d / (k_d + k_f). \quad (3)$$

Once the e–h pair gets dissociated, the free charge carriers will move toward the respective electrodes, contributing current to the circuit. The electron or hole current density J_n or J_p has two contributions: the drift current due to the electrostatic potential gradient and the diffusion current due to the charge density gradient as described by the following equations

$$\begin{aligned} J_n &= -qn\mu_n \frac{\partial \psi}{\partial x} + qD_n \frac{\partial n}{\partial x} \quad \text{and} \\ J_p &= -qp\mu_p \frac{\partial \psi}{\partial x} - qD_p \frac{\partial p}{\partial x}, \end{aligned} \quad (4)$$

where q is the elementary charge, n or p is the electron or hole density, carrier diffusion coefficients $D = \mu k_B T / q$ [19], μ is the charge carrier mobility and ψ is the electrostatic potential. Also, ψ , n and p satisfy the Poisson equation

$$\frac{\partial^2 \psi}{\partial x^2} = \frac{q}{\epsilon} (n - p), \quad (5)$$

where ϵ is the dielectric constant.

Electrons and holes could recombine during the transport of free charge carriers. The bimolecular recombination is one of the most crucial charge carrier loss mechanisms which limit the photocurrent, though there is possible loss through charge traps. The bimolecular recombination rate R is given by

$$R = k_r (np - n_{\text{int}}^2), \quad (6)$$

where the bimolecular recombination rate constant determined by the minimum mobility is given by $k_r = \frac{q}{\epsilon} \min(\mu_n, \mu_p)$, and the intrinsic carrier density of electrons or holes $n_{\text{int}} = N_c \exp(-qE_{\text{gap}}/k_B T)$, where N_c is the effective density of states at either conduction or valence band edge, E_{gap} is the effective band gap between the lowest unoccupied molecular orbital (LUMO) of the acceptor and the highest occupied molecular orbital (HOMO) of the donor, k_B is Boltzmann's constant and T is the absolute temperature.

The net generation of free charge carriers depends on generation of the e–h pair and its subsequent dissociation and decay. In the steady state, the number X of bound e–h pairs per unit volume changes with time as

$$\frac{dX}{dt} = G - k_f X - k_d X + R = 0, \quad (7)$$

where G is the generation rate of an e–h pair, k_d is the dissociation rate, and k_f is the decay rate of bound e–h pairs. Utilizing Eq. 3 and Eq. 7, the net generation rate U of free charge carriers can be written as

$$U = k_d X - R = PG - (1 - P)R, \quad (8)$$

where P is the probability of e–h pair dissociation defined by Eq. 3. Here, U is related to the gradient of current density J through the continuity equations

$$\frac{\partial}{\partial x} J_n = qU \quad \text{and} \quad \frac{\partial}{\partial x} J_p = -qU. \quad (9)$$

To obtain the solution of the continuity and Poisson equations, boundary conditions of charge densities and electrostatic potential need to be supplied. The effective electron and hole densities at the respective electrode, N_c , give the boundary condition for carrier densities. The effective band gap E_{gap} sets the boundary condition for the electrostatic potential as

$$\psi(0) - \psi(L) = E_{\text{gap}}/q - V_a, \quad (10)$$

where L is the device thickness, and V_a is the applied external voltage. With the appropriate boundary conditions, the Poisson and continuity equations can be solved iteratively by a numerical scheme proposed by Gummel [39, 40]. Finally, the J – V curve and carrier density distributions are obtained. The device structure and the flow chart of the simulation program are depicted in Fig. 1.

The separation of bound e–h pairs into free charges is an important process in the BHJ solar cells [41]. The photocurrent is governed by the dissociation of e–h pairs, which is field and temperature dependent according to Onsager's theory [42]. Braun has made an important refinement to this theory by pointing out that the bound e–h pair has a

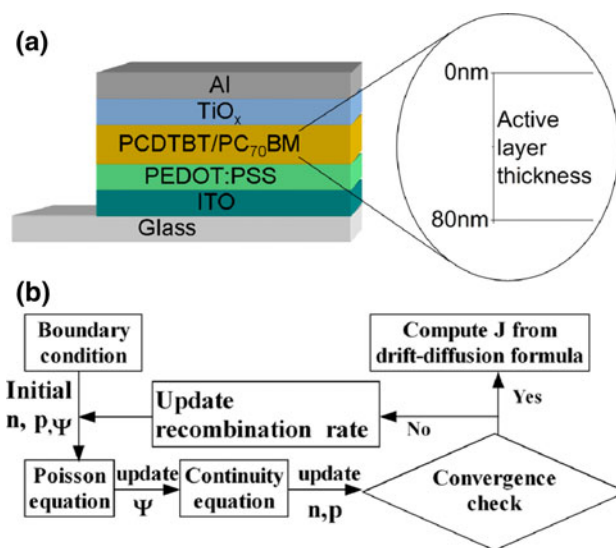


Fig. 1 **a** Device structure of the BHJ solar cells, taking the low band gap polymer PCDTBT/PC₇₀BM as example; **b** flow chart of the device model simulation process. It starts with an initial guess for the potential and carrier densities. The steady state is obtained by solving the Poisson and continuity equations iteratively with a convergence criterion of 10^{-7} [64]

finite lifetime [38]. Therefore, the dissociation rate k_d can be calculated by

$$k_d = \frac{3R}{4\pi a^3} e^{-E_b/k_B T} \left(1 + b + \frac{b^2}{3} + \dots \right), \quad (11)$$

where R is the Langevin bimolecular recombination rate, a is the electron–hole pair distance, E_b is the e–h pair binding energy $\sim q^2/(4\pi\epsilon a)$, and $b = q^3 F / (8\pi\epsilon k_B^2 T^2)$, F is the field strength. Recently, Wojcik and Tachiya have developed an extended Onsager theory [43] based on the finite recombination rate at a nonzero reaction radius. They claimed that Braun's model was based on the assumption that both recombination and separation processes follow exponential kinetics, which might not be true.

The classical bimolecular recombination Langevin formalism was reported in 1903 [44]. After that, several models have been proposed in literatures to explain the recombination mechanism. These models are outlined as follows: (1) the classical Langevin model [44] with the recombination rate constant $k_r = \frac{q}{\epsilon}(\mu_n + \mu_p)$; (2) the minimum mobility model [45] where the recombination rate constant is given by $k_r = \frac{q}{\epsilon} \min(\mu_n, \mu_p)$; (3) the potential fluctuation model [46] where a potential barrier ΔE proportional to the band energy fluctuations has to be overcome before recombination, $k_r = \frac{q}{\epsilon} \exp\left(-\frac{\Delta E}{k_B T}\right)(\mu_n + \mu_p)$; (4) the carrier concentration gradient model [47] in which the recombination rate is proportional to the local product of electron and hole concentrations; (5) the two-dimensional Langevin recombination theory [48] where the recombination rate depends on the square root of the density of charge carriers; and (6) the unified theory of geminate and bulk electron–hole recombination [49] where the recombination occurs at a nonzero separation with a finite intrinsic rate to account for the observed much smaller recombination rate constant than that predicted from the Langevin theory.

Since the one-dimensional drift–diffusion model can only be applied to the BHJ or bilayer system described by the one-dimensional density fluctuation across the active layer, an extension of the device model to higher dimensions is needed to account for the impact of morphology. Buxton and Clarke [25, 50] developed a two-dimensional device model to simulate the morphological influence such as domain size, order, and percolation, on the J – V curve and other device properties. The dissociation probability of e–h pairs through which free charge carriers are created is not properly treated in their model and the photogeneration of excitons has been assumed to follow exponential dependence on the distance from the top electrode. Williams and Walker [51] presented a two-dimensional model in which the effects of optical interference and the competition between dissociation and decay of e–h pairs were included. Maturova et al. [27, 28, 30]

also developed a two-dimensional morphological model. In the model, the active layer is divided into two regions, the so-called donor–acceptor mix and acceptor pure phases. Since the precise location of charge separation is not specified, it is difficult to establish a quantitative relationship between the performance of solar cells and the degrees of phase separation with this model.

On the other hand, such equilibrium device models can only give a description of the steady-state behavior. Hwang and Greenham [26] utilized a time-dependent device model to deal with the transient photocurrent of organic BHJ solar cells. The simulated transient photocurrent well reproduced the experimental results. They later improved the time-dependent device model by incorporating the electron trapping [29].

2.2 Dynamic Monte Carlo model

Watkins et al. [52] first developed a dynamic Monte Carlo model to investigate the dependence of IQE on the scale of phase separation. This model focuses on the IQE, not the J – V curve, and several important characteristics of the organic solar cells, including J_{SC} , V_{OC} , and FF, have been completely ignored. To improve the description of charge carrier behavior, Marsh et al. [53] designed a model taking into account dark injection at the electrodes; however, the exciton creation, diffusion, and dissociation have been ignored in their model, only charge transport in the organic nanostructures is considered. Yang and Forrest [54] developed a model where effects of optical interference and exciton and carrier transport were considered. The model focuses on the external quantum efficiency EQE without considering the J_{SC} , V_{OC} , and PCE of the solar cells. The authors of this account and collaborators [55] have incorporated all the microscopic processes of exciton and charge carrier dynamics in the modeling, to obtain the absolute power conversion efficiency of organic solar cells. The scheme of this simulation process [55] is shown in Fig. 2.

Firstly, the relation between the scale of phase separation and the device performance is of interest. In order to obtain a series of BHJ morphologies with varying scales of phase separation, an entropy-driven site spin exchange Ising model is often employed [52–55] with parameters adjusted to reproduce the observed grain sizes and distribution for binary phase mixtures [56, 57]. Apart from the Ising model, Frost et al. [58] developed a polymer chain model. By altering the interaction energies between the polymer chains, various polymer film morphologies were generated.

In the Ising model, the DA phase morphology is described by a three-dimensional array of lattice sites. Each site is occupied either by a donor or an acceptor, which corresponds to spin up or down, respectively. The Ising Hamiltonian for site i is

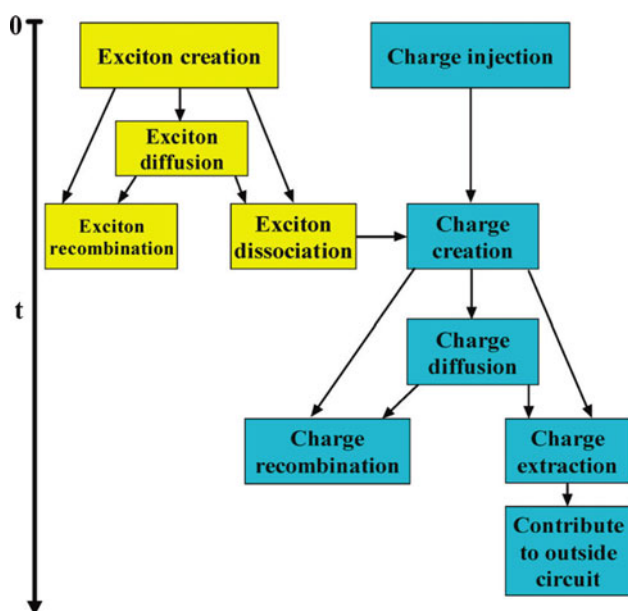


Fig. 2 Scheme of the dynamic Monte Carlo simulation processes, incorporating both exciton and charge carrier dynamics [55]

$$\varepsilon_i = -\frac{J}{2} \sum_j (\delta_{s_i s_j} - 1), \quad (12)$$

where $\delta_{s_i s_j}$ is the delta function, and s_i and s_j are the spins of sites i and j . The summation over j includes all the first- and second-nearest neighbors of site i , and the coupling constant J is inversely proportional to the distance between sites i and j , *i.e.*, the energetic contribution is scaled by a factor of $1/\sqrt{2}$ for the second-nearest neighbors. To obtain a series of morphologies with varying phase interpenetrations, we need to decide the appropriate initial configuration. In the simulation, the initial morphology is chosen with the minimal phase separation and J is set to unity. To relax the system to an energetically favorable state, a neighboring pair of sites is chosen randomly in the system, and the acceptance probability for an attempt to swap the site spins is calculated as

$$P(\Delta\varepsilon) = \frac{\exp(-\Delta\varepsilon/k_B T)}{1 + \exp(-\Delta\varepsilon/k_B T)}, \quad (13)$$

where $\Delta\varepsilon$ is the total energy change in the system caused by swapping the two spins. After a large number of swapping, a series of BHJ morphologies with varying scales of phase separation can be generated. The bilayer and regular checkerboard morphologies [59, 60] are also chosen as special cases for comparison, see Fig. 3.

To model the photovoltaic devices, the movement and interactions of an ensemble of particles including excitons, electrons, and holes are tracked explicitly by the dynamic Monte Carlo (DMC) method. An algorithm particularly suitable for the problem at hand is the first reaction method (FRM) [61–63]. In the FRM description, each of these

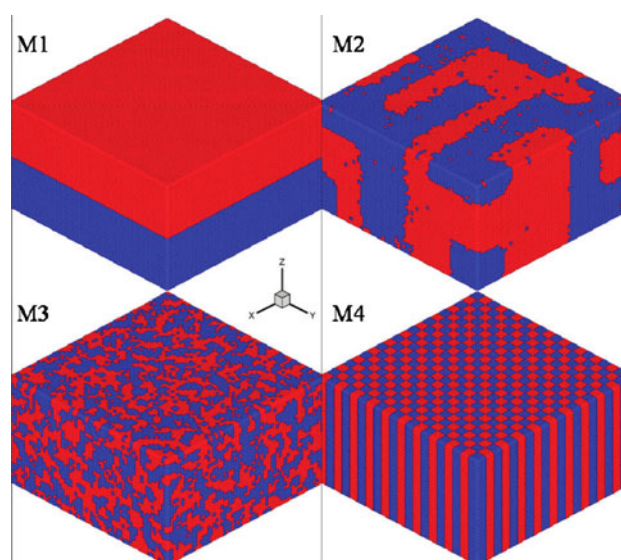


Fig. 3 Typical morphologies with different scales of phase separation, M1 for the bilayer, M2 and M3 for the BHJ morphologies generated by the Ising model, and M4 for the checkerboard structure. The electron and hole conductors are colored with red and blue, respectively [55]

particles is associated with an event, and each event has a waiting time, τ_q . An event is usually associated with a configurational change in the system, for instance, inserting or removing a particle or updating the coordinates of the particles. All the possible events are stored in the order of ascending waiting times and form a temporal sequence. This queue of events will be constantly updated to reflect the time evolution of the system. At each time step, the event at the start of the queue is executed and removed from the queue. The simulation time is incremented by the time spent and all the waiting times in the queue are reduced by this time period. The execution of the current event will probably preclude the occurrence of subsequent events, and it will also enable new event to be created and inserted in the queue.

The waiting time τ_q is calculated as

$$\tau_q = -\frac{1}{W} \ln(Y), \quad (14)$$

where Y is a random number uniformly distributed between 0 and 1 and W is the occurring rate (in s^{-1}) of the event. For each particle, only the event with the shortest waiting time needs to be inserted in the queue. As a result, we need to calculate the waiting times for all possible events associated with a particular particle and insert the event with the smallest waiting time for the particle into the queue.

3 Modeling BHJ photovoltaic device performance

Recently, our group has applied both the continuum device model and the DMC methods to simulate the photovoltaic

performance of BHJ solar cells, namely, the open-circuit voltage, the short-circuit current, the internal quantum efficiency, and the power-conversion efficiency. Our primary objective is to establish a quantitative relationship between the device performance and the morphology and microscopic processes such as charge dissociation and recombination as well as charge mobilities.

3.1 Open-circuit voltage V_{OC}

Highly efficient BHJ photovoltaic cells with poly [N-9'-hepta-decanyl-2,7-carbazole-alt-5,5-(4',7'-di-2-thienyl-2',1',3'-benzothiadiazole)] (PCDTBT) as the donor and [6]-phenyl C₇₀-butyric acid methyl ester (PC₇₀BM) as the acceptor (see Fig. 4) have been reported recently [12]. The PCDTBT/PC₇₀BM solar cells exhibit one of the best performances of organic solar cells studied to date, with the PCE 6.1% and the V_{OC} as high as 0.88 V. We have performed numerical simulations on the PCDTBT/PC₇₀BM solar cells with the one-dimensional continuum device model.

Both the experimental and simulated J - V curves under the illumination of monochromatic green light (532 nm) as well as AM 1.5 G irradiation are shown in Fig. 5 for comparison [64]. The good agreement between the experiment and the simulation justifies the model adopted in our investigation and the underlying mechanisms incorporated. The parameters used in the simulation are listed in Table 1.

In Fig. 6, the influence of light intensity on V_{OC} is shown. The V_{OC} is found to exhibit a linear dependence on the logarithm of light intensity. The fitted slope, 0.026 V, is close to the experimental data ~ 0.03 V reported by Tromholt et al. [65] and is consistent with the theoretical

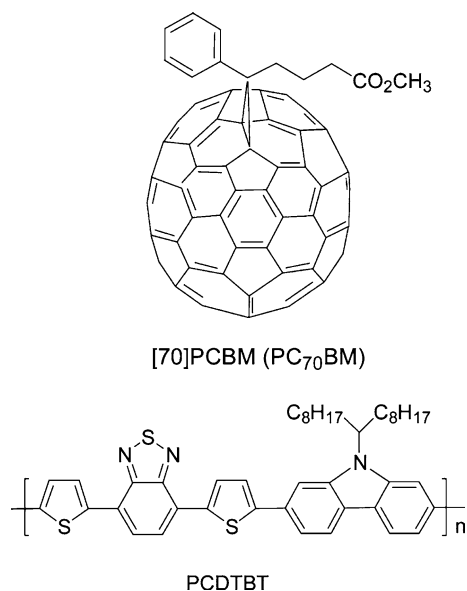


Fig. 4 The chemical structures of PC₇₀BM and PCDTBT

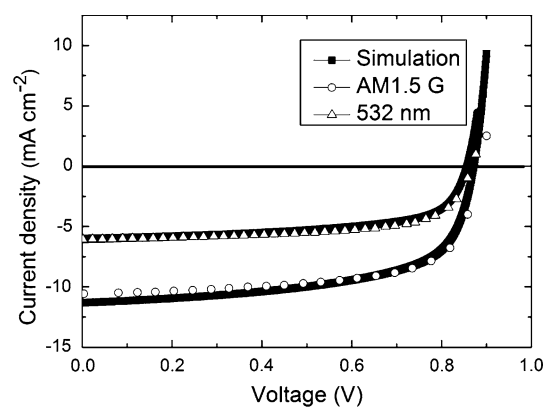


Fig. 5 Comparison between the simulated and experimental J - V curves for the PCDTBT/PC₇₀BM device. Two types of illumination condition are considered, AM 1.5 G and monochrome at 532 nm. Both manifest a very nice fit with a single set of parameters [64]

Table 1 Overview of the parameters used to obtain the simulation results shown in Fig. 5

Parameter	Symbol	Numerical value
Band gap	E_{gap}	1.3 eV
Electron mobility	μ_n	$3.5 \times 10^{-7} \text{ m}^2/\text{V s}$
Hole mobility	μ_p	$1.0 \times 10^{-7} \text{ m}^2/\text{V s}$
Eff. density of states	N_C	$2.5 \times 10^{25} \text{ m}^{-3}$
Generation rate	G	$1 \times 10^{28} \text{ m}^{-3} \text{ s}^{-1}$
Dielectric constant	ϵ	3.5
e-h pair distance	a	1.6 nm
Decay rate	k_f	$1.5 \times 10^6 \text{ s}^{-1}$

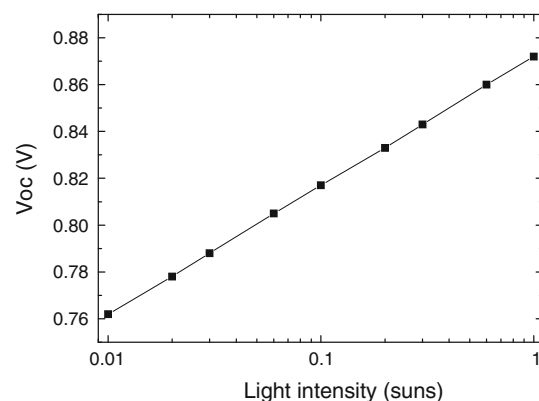


Fig. 6 Light intensity dependence of V_{OC} simulated by the continuum device model for the PCDTBT/PC₇₀BM device

prediction based on the notion that the quasi-Fermi levels are constant throughout the device, as pointed out by Koster et al. [66]

$$V_{oc} = \frac{E_{\text{gap}}}{q} - \frac{k_B T}{q} \ln \frac{(1-P)k_r N_c^2}{PG}, \quad (15)$$

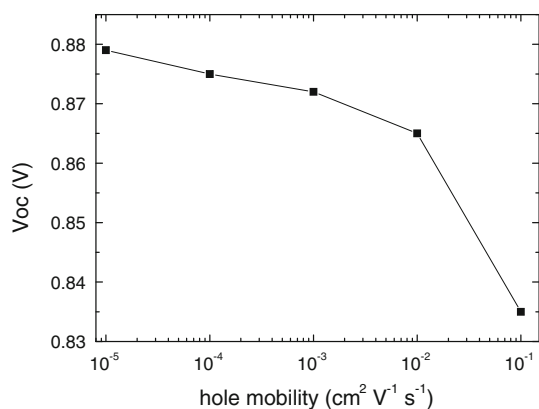


Fig. 7 V_{OC} as a function of hole mobility μ_p (the electron mobility μ_n is taken as $3.5 \times \mu_p$) simulated with the continuum device model for the PCDTBT/PC₇₀BM system

where P is the probability of e–h pair dissociation defined by Eq. 3, k_r is the bimolecular recombination rate constant, N_c is the effective density of states at either conduction or valence band edge and G is the generation rate of an e–h pair. Eq. 15 shows that V_{OC} is proportional to the logarithm of G , or light intensity.

Furthermore, we studied the effect of charge carrier mobilities on V_{OC} as shown in Fig. 7. It is found that increase in mobility leads to reduction of V_{OC} . Since recombination is a key loss mechanism in organic solar cells and the bimolecular recombination rate constant $k_r = \frac{\epsilon}{q} \mu$ is proportional to the mobilities, high mobilities thus result in high recombination rate. Hence, the electron and hole densities are reduced when large numbers of free charge carriers recombine during transport.

In BHJ organic solar cells, V_{OC} can be defined from the quasi-Fermi level splitting as [67–69]

$$qV_{OC} = E_{\text{gap}} - k_B T \ln \left(\frac{N_L N_H}{np} \right), \quad (16)$$

> 0

where N_L and N_H are the densities of states of the LUMO of acceptor and the HOMO of donor, respectively [66], which cannot be exceeded by the electron and hole densities n and p in the device. According to Eq. 16, we know that V_{OC} decreases with reduced charge carrier densities. The trend observed is also consistent with the work by Mandoc et al. [70] and Deibel et al. [71].

We also investigated the k_d and k_f dependence of V_{OC} [64]. Figure 8 shows that increasing k_d and decreasing k_f could lead to enhancement of V_{OC} . For $V_{OC} > 0.9$ V, which corresponds to the regime of $k_d > 4k_f$, 79% of the bound e–h pairs dissociate into free charge carriers without significant decay to the ground state. In this case, a large number of free charge carriers can participate in the

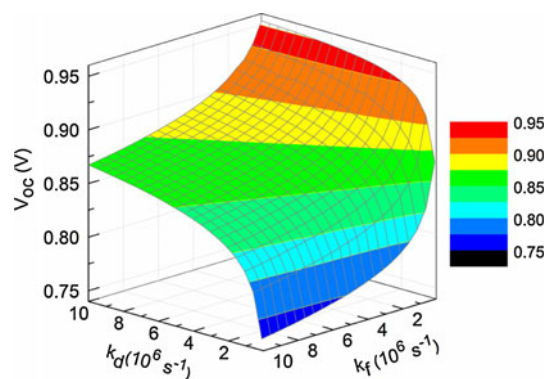


Fig. 8 Influence of the dissociate rate k_d and the decay rate k_f on the open-circuit voltage V_{OC} of the PCDTBT/PC₇₀BM solar cells simulated by the continuum device model [64]

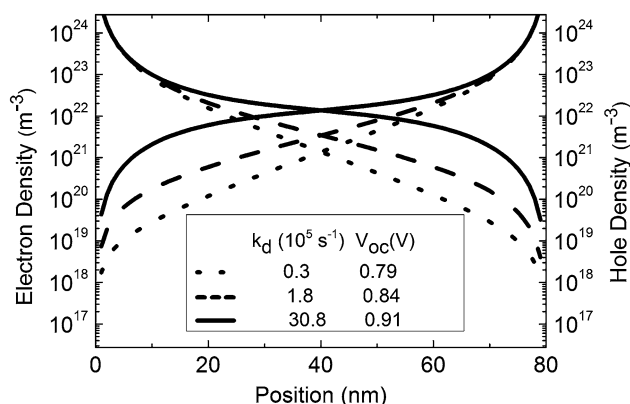


Fig. 9 Electron and hole density distributions in the PCDTBT/PC₇₀BM device for various dissociation rates k_d at fixed $k_f = 5 \times 10^5 \text{ s}^{-1}$ under the open-circuit condition [64]

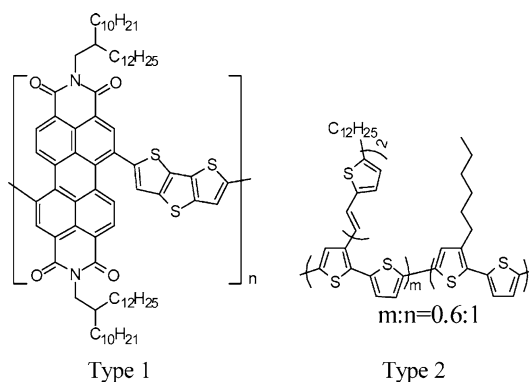
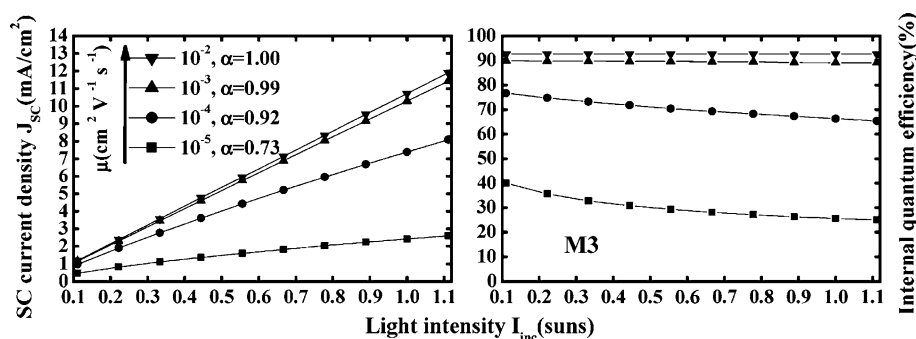


Fig. 10 The chemical structures of poly(perylene diimide-alt-dithienothiophene) (PPDI) and bis(thienylenevinylene)-substituted polythiophene (PBTT) [72, 73]

transport and reach the electrodes. We show in Fig. 9 the electron and hole density distributions for various k_d at fixed $k_f = 5 \times 10^5 \text{ s}^{-1}$. It can be seen that as k_d increases the amount of electron–hole pairs which decay in the bulk

Fig. 11 The dependence of J_{SC} and IQE on the mobility and the light intensity for the morphology M3, obtained with the DMC model. J_{SC} is related to the light intensity I as $J_{SC} \propto I^\alpha$, and α varies with the mobility [55]



reduces dramatically. The high k_d and low k_f values will lead to high values of n and p , and as a result increased V_{OC} according to Eq. 16. This is fully in line with the simulation results shown in Fig. 9. In another extreme case, for $k_d < 0.071k_f$, Fig. 8 shows that $V_{OC} < 0.8$ V. Under such situations, only 6.6% of electron–hole pairs dissociate into free charge carriers, most of them decay to the ground state. This means that the electron (hole) density within the device is low. Thus, the open-circuit voltage is consequently low according to Eq. 16.

3.2 Short-circuit current density J_{SC} and internal quantum efficiency IQE

Recently, Zhan et al. [72] reported experimental studies on the all-polymer BHJ solar cells based on a new solution-processible conjugated polymer poly(perylene diimide-alt-dithienothiophene) (PPDI) and bi(thienylenevinylene)-substituted polythiophene [73] (PBTT) as shown in Fig. 10. This is full polymer blend solar cell which exhibits the highest power-conversion efficiency $\sim 1.5\%$. Starting from the experimental parameters, we performed dynamic Monte Carlo simulations on the PPDT/PBTT solar cell and found that if both morphology and charge mobilities are optimized, the PCE can reach as high as 5% for this type of device [55]. The DMC method and our improvement have been described in Sect. 2.2. Below, we simply present the simulation results.

Figure 11 shows that the simulated J_{SC} increases sub-linearly with the light intensity or exciton creation rate. However, when the charge mobility is over 10^{-3} $\text{cm}^2 \text{V}^{-1} \text{s}^{-1}$, the J_{SC} and the IQE are no longer sensitive to the mobility [55]. Higher light intensity results in more excitons and e–h pairs; therefore, more free charge carriers move to the electrodes and contribute to the photocurrent. When the mobility is high enough, most of the carriers can move rapidly toward the electrodes; as a result, a further increase in mobility does not significantly improve the device's performance due to the steady current requirement and fixed photogenerated charges. This observation is also confirmed by our simulations with the continuum device

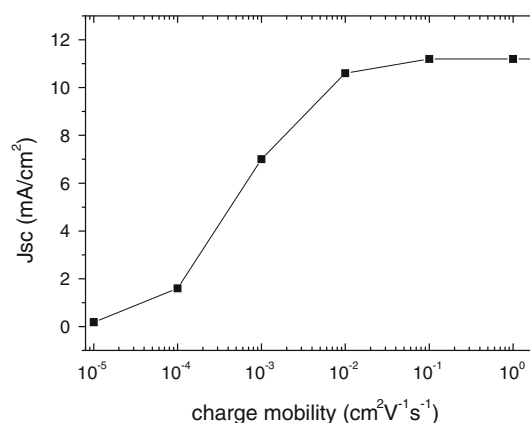


Fig. 12 J_{SC} as a function of charge carrier mobility calculated by the continuum device model for the all-polymer device

model (Fig. 12) where J_{SC} is found not further improved when the mobility is over $\sim 10^{-2}$ $\text{cm}^2 \text{V}^{-1} \text{s}^{-1}$.

The IQE and its two constituents, the exciton dissociation efficiency (the ratio of the number of excitons dissociated with respect to the number of excitons generated) and charge collection efficiency (the ratio of the net number of charges collected by the electrodes to twice of the number of excitons dissociated), were calculated for various morphologies including the checkerboard morphology using the dynamic Monte Carlo model (Fig. 13) [55]. For morphologies with phase separation, large feature size means small interfacial area between DA phases and low exciton-dissociation efficiency, but high charge-collection efficiency; in contrast for small feature size, exciton-dissociation efficiency is increased but charge-collection efficiency is decreased. For a series of morphologies studied, peak IQE corresponds to the optimal nanostructure size of around 10 nm, whereas for the checkerboard, the maximum IQE occurs when the domain size is around 9 nm.

3.3 Power-conversion efficiency PCE

The PCE contour curves obtained with the dynamic Monte Carlo model [55] are plotted in Fig. 14. It shows that up to 5% PCE can be achieved for the optimal charge mobility combined with the optimal film morphology, while the

Fig. 13 For the BHJ and checkered morphologies, exciton dissociation efficiency, charge collection efficiency, and IQE vary with the interfacial area between the electron and hole conductors [55]

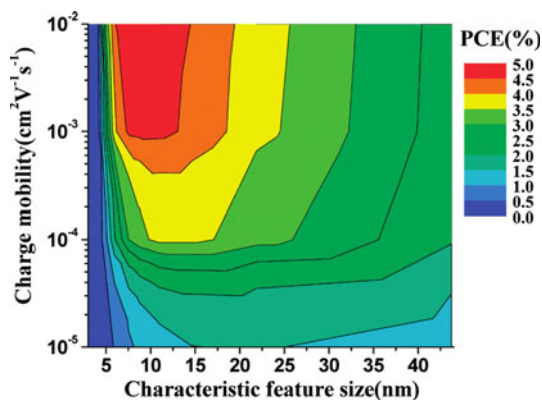
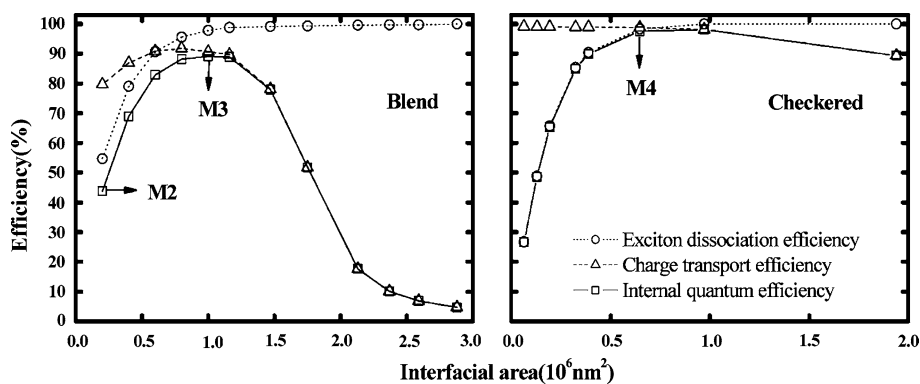


Fig. 14 Contour plots showing the PCE versus the charge mobility and the characteristic feature size of the BHJ morphologies obtained with the dynamic Monte Carlo model for the all-polymer device. The V_{OC} and FF used in the calculation are 0.63 V and 0.65, respectively [55]

current experimental measurement gives a PCE of about 1.5%, indicating that there is still room to improve the PCE for such full polymer devices. It is worth noting that the polymer/fullerene device performs much better than the all-polymer solar cell.

As an independent check, we use the continuum device model to study the same all-polymer solar cell. In Fig. 15, it is observed that the PCE exhibits a distinct maximum of a bit larger than 5%. The peak PCE value corresponds to the mobility of around $10^{-1} \text{ cm}^2 \text{ V}^{-1} \text{ s}^{-1}$, which is in good agreement with those reported in the literatures [70, 71]. With very high mobilities, the reduced concentration of charge carriers decreases the V_{OC} , and the J_{SC} is saturated as explained earlier therefore the PCE is decreased, whereas at low mobilities, the loss in J_{SC} (see Eq. 4) is responsible for the decrease of the PCE.

4 Conclusions and perspectives

To conclude, in this account we introduce two computational models proposed for modeling the BHJ solar cells

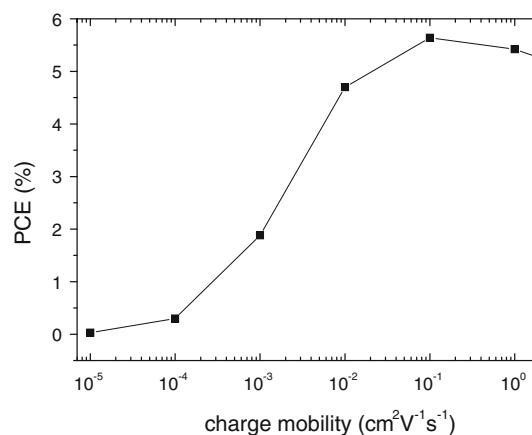


Fig. 15 The dependence of PCE on the charge mobility, simulated by the continuum device model for the all-polymer solar cells

and extensively used in analyzing the photovoltaic properties. The continuum device model focuses on the macroscopic quantities, while the dynamic Monte Carlo model focuses on microscopic particle behaviors. We have applied the two models to simulating the organic photovoltaic devices and studying the influence of mobilities, dissociation and decay rates of bound e-h pairs, and domain sizes on the device performance. The results obtained from these simulations have provided strategies for further improving the device efficiencies. However, there exist drawbacks in the current models, for instance, the device model cannot explicitly account for the phase separation of the blend. The DMC model does account for the morphological effect, but in a crude manner. Moreover, the DMC model cannot fully describe the J - V characteristics, especially the dependence of V_{OC} on the light intensity, mobility, and morphology. So studies using the DMC model are often focused on one or a few aspects of the devices, such as IQE and EQE. As a result, we recommend the two-dimensional even three-dimensional continuum device model be developed to investigate the morphological effect as well as the dynamic Monte Carlo model coupled with the Poisson equation to account for the

space-charge effect. On the other hand, compared with the Ising model utilized here to generate morphologies for use in the later DMC simulations, local properties of the interfaces have been studied in more detail by means of quantum–mechanical calculations [74]. These sophisticated methods should be employed in the modeling of organic photovoltaic devices. Our future effort on the theoretical characterization of the organic solar cells will be along the above directions.

Acknowledgments Collaborations with Prof. Alison Walker of University of Bath on the dynamic Monte Carlo simulations are greatly acknowledged. Extensive discussions with Prof. Xiaowei Zhan and Prof. Yongfang Li have been very helpful. This work was supported by the National Natural Science Foundation of China (grant nos. 20920102031, and 20903060) and the Ministry of Science and Technology of China through 973 program.

References

- Coakley KM, McGehee MD (2004) *Chem Mat* 16:4533
- Peet J, Senatore ML, Heeger AJ, Bazan GC (2009) *Adv Mater* 21:1521
- Krebs FC (2009) *Sol Energy Mater Sol Cells* 93:394
- Sariciftci NS, Smilowitz L, Heeger AJ, Wudl F (1992) *Science* 258:1474
- Yu G, Gao J, Hummelen JC, Wudl F, Heeger AJ (1995) *Science* 270:1789
- Halls JJM, Walsh CA, Greenham NC, Marseglia EA, Friend RH, Moratti SC, Holmes AB (1995) *Nature* 376:498
- Kim JY, Lee K, Coates NE, Moses D, Nguyen TQ, Dante M, Heeger AJ (2007) *Science* 317:222
- Tang CW (1986) *Appl Phys Lett* 48:183
- Po R, Maggini M, Camaioni N (2010) *J Phys Chem C* 114:695
- Chamberlain GA (1983) *Solar Cells* 8:47
- Nunzi JM (2002) *C R Phys* 3:523
- Park SH, Roy A, Beaupre S, Cho S, Coates N, Moon JS, Moses D, Leclerc M, Lee K, Heeger AJ (2009) *Nat Photonics* 3:297
- Liang YY, Xu Z, Xia JB, Tsai ST, Wu Y, Li G, Ray C, Yu LP (2010) *Adv Mater* 22:E135
- Chen HY, Hou JH, Zhang SQ, Liang YY, Yang GW, Yang Y, Yu LP, Wu Y, Li G (2009) *Nat Photonics* 3:649
- Scharber MC, Wuhlbacher D, Koppe M, Denk P, Waldauf C, Heeger AJ, Brabec CL (2006) *Adv Mater* 18:789
- Koster LJA, Mihailetchi VD, Blom PWM (2006) *Appl Phys Lett* 88:093511
- Dennler G, Scharber MC, Ameri T, Denk P, Forberich K, Waldauf C, Brabec CJ (2008) *Adv Mater* 20:579
- Sun SS, Sariciftci NS (2005) *Organic photovoltaics: mechanisms, materials, and devices*. Taylor & Francis Group, Boca Raton
- Selberherr S (1984) *Analysis and simulation of semiconductor devices*. Springer, New York
- Crone BK, Davids PS, Campbell IH, Smith DL (2000) *J Appl Phys* 87:1974
- Ruhstaller B, Carter SA, Barth S, Riel H, Riess W, Scott JC (2001) *J Appl Phys* 89:4575
- Gregg BA, Hanna MC (2003) *J Appl Phys* 93:3605
- Barker JA, Ramsdale CM, Greenham NC (2003) *Phys Rev B* 67:075205
- Koster LJA, Smits ECP, Mihailetchi VD, Blom PWM (2005) *Phys Rev B* 72:085205
- Buxton GA, Clarke N (2006) *Phys Rev B* 74:085207
- Hwang I, Greenham NC (2008) *Nanotechnology* 19:424012
- Maturova K, Kemerink M, Wienk MM, Charrier DSH, Janssen RAJ (2009) *Adv Funct Mater* 19:1379
- Maturova K, van Bavel SS, Wienk MM, Janssen RAJ, Kemerink M (2009) *Nano Lett* 9:3032
- Hwang I, McNeill CR, Greenham NC (2009) *J Appl Phys* 106:094506
- Maturova K, Janssen RAJ, Kemerink M (2010) *ACS Nano* 4:1385
- Shieh JT, Liu CH, Meng HF, Tseng SR, Chao YC, Horng SF (2010) *J Appl Phys* 107:084503
- Nam YM, Huh J, Jo WH (2010) *Sol Energy Mater Sol Cells* 94:1118
- Morteani AC, Sreearunothai P, Herz LM, Friend RH, Silva C (2004) *Phys Rev Lett* 92:247402
- De S, Pascher T, Maiti M, Jespersen KG, Kesti T, Zhang FL, Inganas O, Yartsev A, Sundstrom V (2007) *J Am Chem Soc* 129:8466
- Veldman D, Ipek O, Meskers SCJ, Sweelssen J, Koetse MM, Veenstra SC, Kroon JM, van Bavel SS, Loos J, Janssen RAJ (2008) *J Am Chem Soc* 130:7721
- Drori T, Sheng CX, Ndobe A, Singh S, Holt J, Vardeny ZV (2008) *Phys Rev Lett* 101:037401
- Brabec CJ, Sariciftci NS, Hummelen JC (2001) *Adv Funct Mater* 11:15
- Braun CL (1984) *J Chem Phys* 80:4157
- Gummel HK (1964) *IEEE Trans Electron Devices* 11:455
- Scharfettl DI, Gummel HK (1969) *IEEE Trans Electron Devices* 16:64
- Mihailetchi VD, Koster LJA, Hummelen JC, Blom PWM (2004) *Phys Rev Lett* 93:216601
- Onsager L (1934) *J Chem Phys* 2:599
- Wojcik M, Tachiya M (2009) *J Chem Phys* 130:104107
- Langevin P (1903) *Ann Chim Phys* 28:433
- Koster LJA, Mihailetchi VD, Blom PWM (2006) *Appl Phys Lett* 88:052104
- Adriaenssens GJ, Arkhipov VI (1997) *Solid State Commun* 103:541
- Deibel C, Wagenpfahl A, Dyakonov V (2009) *Phys Rev B* 80:075203
- Juska G, Genevicius K, Nekrasas N, Sliuzys G, Osterbacka R (2009) *Appl Phys Lett* 95:013303
- Hilczler M, Tachiya M (2010) *J Phys Chem C* 114:6808
- Buxton GA, Clarke N (2007) *Model Simul Mater Sci Eng* 15:13
- Williams J, Walker AB (2008) *Nanotechnology* 19:424011
- Watkins PK, Walker AB, Verschoor GLB (2005) *Nano Lett* 5:1814
- Marsh RA, Groves C, Greenham NC (2007) *J Appl Phys* 101:083509
- Yang F, Forrest SR (2008) *ACS Nano* 2:1022
- Meng LY, Shang Y, Li QK, Li YF, Zhan XW, Shuai ZG, Kimber RGE, Walker AB (2010) *J Phys Chem B* 114:36
- Adams CD, Srolovitz DJ, Atzmon M (1993) *J Appl Phys* 74:1707
- Peumans P, Uchida S, Forrest SR (2003) *Nature* 425:158
- Frost JM, Cheynis F, Tuladhar SM, Nelson J (2006) *Nano Lett* 6:1674
- Gunes S, Neugebauer H, Sariciftci NS (2007) *Chem Rev* 107:1324
- Sun SS (2003) *Sol Energy Mater Sol Cells* 79:257
- Gillespie DT (1976) *J Comput Phys* 22:403
- Jansen APJ (1995) *Comput Phys Commun* 86:1
- Lukkien JJ, Segers JPL, Hilbers PAJ, Gelten RJ, Jansen APJ (1998) *Phys Rev E* 58:2598
- Shang Y, Li Q, Meng L, Wang D, Shuai Z (2010) *Appl Phys Lett* 97:143511
- Tromholt T, Katz EA, Hirsch B, Vossier A, Krebs FC (2010) *Appl Phys Lett* 96:073501

66. Koster LJA, Mihailetschi VD, Ramaker R, Blom PWM (2005) *Appl Phys Lett* 86:123509
67. Brabec CJ, Cravino A, Meissner D, Sariciftci NS, Fromherz T, Rispens MT, Sanchez L, Hummelen JC (2001) *Adv Funct Mater* 11:374
68. Würfel P (2004) *Physics of solar cells: from principles to new concepts*. Wiley-VCH, Weinheim
69. Riede M, Mueller T, Tress W, Schueppel R, Leo K (2008) *Nanotechnology* 19:424001
70. Mandoc MM, Koster LJA, Blom PWM (2007) *Appl Phys Lett* 90:133504
71. Deibel C, Wagenpfahl A, Dyakonov V (2008) *Phys Status Solidi-Rapid Res Lett* 2:175
72. Zhan XW, Tan ZA, Domercq B, An ZS, Zhang X, Barlow S, Li YF, Zhu DB, Kippelen B, Marder SR (2007) *J Am Chem Soc* 129:7246
73. Hou JH, Tan ZA, Yan Y, He YJ, Yang CH, Li YF (2006) *J Am Chem Soc* 128:4911
74. Yi YP, Coropceanu V, Bredas JL (2009) *J Am Chem Soc* 131:15777